RESEARCH

Dissociation of the nuclear WWOX/TRAF2 switch renders UV/cold shock-mediated nuclear bubbling cell death at low temperatures

Szu-Jung Chen[1†], Cheng-Chang Tsai[1†], Sing-Ru Lin[1], Ming-Hui Lee[1], Shenq-Shyang Huang[1], Han-Yan Zeng[2], Lu-Hai Wang[3], Ming-Fu Chiang[4*], Hamm-Ming Sheu[5*] and Nan-Shan Chang[1,2*]

Abstract

Background Normal cells express functional tumor suppressor WW domain-containing oxidoreductase (WWOX), designated WWOXf. UV irradiation induces WWOXf cells to undergo bubbling cell death (BCD) — an event due to the accumulation of nuclear nitric oxide (NO) gas that forcefully pushes the nuclear and cell membranes to form one or two bubbles at room temperature (22 °C) and below. In contrast, when WWOX-deficient or -dysfunctional (WWOXd) cells are exposed to UV and/or cold shock, the cells undergo nuclear pop-out explosion death (POD). We aimed to determine the morphological and biochemical changes in WWOXf cells during BCD versus apoptosis.

Methods WWOXf and WWOXd cells were exposed to UV followed by measuring BCD or POD by time-lapse microscopy and/or time-lapse holographic microscopy at 4, 22, or 37 °C to visualize morphological changes. Live cell stains were used to measure the kinetics of nitric oxide (NO) production and Ca^{2+} influx. Extent of cell death was measured by uptake of propidium iodide and by internucleosomal DNA fragmentation using agarose gel electrophoresis.

Results WWOXf cells were exposed to UV and then cold shock, or cold shock and then UV, and cultured at 4, 10, and 22 °C, respectively. Initially, UV induced calcium influx and NO production, which led to nuclear bubbling and final death. Cold shock pretreatment completely suppressed UV-mediated bubbling at 37 °C, so the UV/cold shock-treated cells underwent apoptosis. Without cold shock, UV only induced bubbling at all temperatures, whereas the efficiency of bubbling at 37 °C was reduced by greater than 50%. Morphologically, the WWOXf cell height or thickness was significantly increased during cell division or apoptosis, but the event did not occur in BCD. In comparison, when WWOXd cancer cells received UV or UV/cold shock, these cells underwent NO-independent POD. UV/ cold shock effectively downregulated the expression of many proteins such as the housekeeping α-tubulin (> 70%) and β-actin (< 50%), and cortactin (> 70%) in WWOXf COS7 cells. UV/cold shock induced relocation of α-tubulin to the nucleus and nuclear bubbles in damaged cells. UV induced co-translocation of the WWOX/TRAF2 complex to the nuclei, in which the prosurvival TRAF2 blocked the proapoptotic WWOX via its zinc finger domain. Without WWOX, TRAF2 did not relocate to the nuclei. Cold shock caused the dissociation of the WWOX/TRAF2 complex

†Szu-Jung Chen and Cheng-Chang Tsai contributed equally to this work.

*Correspondence:
Ming-Fu Chiang
chiang66@gmail.com
Hamm-Ming Sheu
hmsheu@mail.ncku.edu.tw
Nan-Shan Chang
wox1world@gmail.com
Full list of author information is available at the end of the article

Chen *et al. Cell Communication and Signaling*   (2024) 22:505

Page 2 of 16

in the nucleus needed for BCD. In contrast, the formation of the WWOX/TRAF2 complex, plus p53, was strengthened at 37 °C required for apoptosis.

Conclusions The temperature-sensitive nuclear WWOX/TRAF2 complex acts as a molecular switch, whose dissociation favors BCD at low temperatures, and the association supports apoptosis at 37 °C in UV-treated WWOXf cells.

Keywords WWOX, UV, Cold shock, TRAF2, Molecular switch, Signaling

Introduction

WW domain-containing oxidoreductase (WWOX), initially identified as a potential tumor suppressor, exhibits dual roles in biological functions. It not only controls the development of the neural system but also prevents neurodegeneration [1–6]. WWOX limits the progression of Alzheimer's disease and other neurodegenerative diseases. Functional deficiency of *WWOX* gene in newborns leads to severe neural disease, seizures, metabolic disorder and early death [3, 4, 7, 8]. *WWOX* gene is a risk factor for Alzheimer's disease [9]. When WWOX is Y33 phosphorylated, pY33-WWOX supports normal physiology, inhibits neurodegeneration, and blocks cancer growth. Conversely, when pY33-WWOX is downregulated, and pS14-WWOX is upregulated, pS14-WWOX supports cancer growth and promotes the progression of Alzheimer's disease [10]. Thus, WWOX exhibits two faces in managing the progression of Alzheimer's disease, cancer growth, and probably other diseases.

In contrast to the programmed cell death [11, 12], we have previously reported nucleus-initiated cell death, designated nuclear-bubbling cell death (BCD) [13, 14]. When the temperature is lowered in the surrounding environment, dying cells do not undergo apoptosis but go through BCD [13, 14]. Our study concerns the severity of frostbite and UV irradiation in the polar regions and even outer space [13, 14]. When exposed to severe cold and strong UV irradiation, people suffer serious damage to their skin. The damage causes further and rapid destruction in internal organs, and eventually leads to limb amputations, organ failure, and even death. BCD was initially defined as "the formation of a single bubble from the nucleus per cell and release of this swelling bubble from the cell surface to extracellular space that irreversibly causes cell death" [13, 14]. When cells are subjected to UV irradiation and/or brief cold shock (4 °C for 5 min) and then incubated at room temperature (22 °C) or 4 °C, each cell releases an enlarging nuclear gas bubble containing nitric oxide (NO) as determined by time-lapse microscopy. Certain cells may simultaneously eject hundreds or thousands of extracellular vesicles (EV) or exosome-like particles. Unlike apoptosis, BCD does not exhibit membrane phosphatidylserine flip-over, mitochondrial apoptosis, damage to the Golgi complex,

and chromosomal DNA fragmentation. BCD stops when the temperature is increased back to 37 °C, and apoptosis starts to proceed [13, 14]. Indeed, BCD can occur to 37 °C. For example, when cells are transiently overexpressed with the Hyal-2/WWOX/Smad4 signaling complex, high-molecular-weight hyaluronan induces BCD at 37 °C [15].

Metastatic cancer cells are frequently deficient in WWOX protein or express dysfunctional WWOX (designated WWOXd) [16, 17]. In response to UV irradiation at 22 °C, WWOXd cells are not efficient in generating calcium (Ca^{2+}) influx, fail to produce nuclear nitric oxide (NO), and ultimately undergo non-apoptotic nuclear explosion or pop-out death (POD). However, UV induces functional WWOX-expressing cells (designated WWOXf) to undergo efficient Ca^{2+} influx, NO production, and then BCD. WWOXf cells migrate collectively and expel the individually migrating WWOXd cells. WWOXd cells in turn induce apoptosis of WWOXf cells from a distance without physical contact [16, 17]. In summary, the research findings highlight the distinct responses of WWOXf and WWOXd cells to UV irradiation, with implications for cancer cell behavior and interaction.

TRAF2 (TNF receptor-associated factor 2) downregulation is a known phenomenon in human skin during frostbite [14]. In this study, we aimed to uncover a novel aspect of cell death mechanisms by investigating the interaction and relocation of WWOX and TRAF2 under UV/cold shock exposure. Our approach, which involved domain mapping by utilizing Förster resonance energy transfer (FRET) imaging, yeast two-hybrid analysis, and cell death assays, led to the discovery of a previously unknown molecular complex that controls UV/cold shock-mediated cell death at low temperatures (22 °C and below) for BCD and 37 °C for apoptosis. These findings represent a significant step forward in our understanding of cell death under extreme conditions.

Materials and methods
Cell lines and chemicals
We used the following WWOXf and WWOXd cell lines [16]. WWOXf cell lines were: 1) African green monkey SV40-transfected kidney COS7 fibroblasts, 2)

Chen *et al. Cell Communication and Signaling*   (2024) 22:505

Page 3 of 16

mouse tumor necrosis factor (TNF)-sensitive L929S fibrosarcoma cells, 3) human colon cancer HCT116 cells, 4) human prostate cancer DU145 cells, 5) human breast MCF7 adenocarcinoma cells [18], 6) human oral squamous cell carcinoma SCC9 and SCC15 cells, and 7) wild type $Wwox^{+/+}$ MEF cells. WWOXd cell lines were: 1) mouse TNF-resistant L929R fibrosarcoma cells, 2) mouse 4T1 mammary carcinoma cells, 3) human neuroblastoma NB69 cells, 4) knockout $Wwox^{-/-}$ MEF cells, 5) mouse NIH-3T3 fibroblasts, and 6) human breast MDA-MB-231 adenocarcinoma cells. MDA-MB-231 cells were from our laboratory (purchased at the American Type Culture Collection (ATCC), Manassas, VA, USA) [16]. Also, MDA-MB-231 (NH) [18] and metastatic MDA-MB-231 (IV2-3) cells were from the National Health Research Institute, Taiwan. MDA-MB-231 and MDA-MB-231 (NH) were considered to come from the exact cell origin. All cell lines were maintained in DMEM medium (Thermo, Waltham, MA, USA) containing 10% heat-inactivated fetal bovine serum (FBS) (Gibco, Billings, MT, USA), except that L929S, L929R, and *Wwox* MEF cells were maintained in RPMI-1640 medium (Sigma, St. Louis, MO, USA) supplemented with 10% heat-inactivated FBS. Cells were incubated at 37℃ with a 5% humidified CO_2 atmosphere.

Chemicals used were 1) propidium iodide (PI), red fluorescent nuclear stain; 2) 4′,6-diamidino-2-phenylindole (DAPI), blue fluorescent nuclear stain; 3) 4-amino-5-methylamino-2′,7′-difluorofluorescein Diacetate (DAF-FM), green fluorescent live cell dye for NO; 4) Fluo-8, green fluorescent calcium-binding dye for live cells; 5) (3-(4,5-dimethylthiazol-2-yl)-2,5-diphenyltetrazolium bromide (MTT): chemical for measuring cell viability via redox potential; 6) betulinic acid [19–22] (the above chemicals #1 to 6 from Sigma-Aldrich, St. Louis, MO, USA); 7) staurosporine [22–24] (LC Laboratories, Boston, MA, USA); 8) caspase inhibitor I (z-VAD-FMK) [25–27]; 9) caspase inhibitor X (specific for caspase 3 and 7) [28–30] (the chemical #8 and 9 from Calbiochem-Merck, Rahway, NJ, USA); 10) Nec-1, inhibitor for RIPK1 {31–34] (Biomol, Hamburg, Germany); 11) GSK'872, inhibitor for RIPK3 [31–34] (Cayman Chemical, Ann Arbor, MI, USA).

cDNA constructs
Mouse *Wwox* cDNA expression constructs were made: 1) WWOX-pECFPC1 [6], 2) EGFP-TRAF2(124–233) [14], and 3) ECFP-TRAF2 [14]. The human full-length TRAF2 cDNA was from ATCC.

Time-lapse bright field and fluorescent microscopy and time-lapse holography
A UV crosslinker (CL-1000 Ultraviolet Crosslinker, UVP, Upland, CA, USA), emitting UVC at 265 nm, was used to irradiate cells at an indicated setting, e.g., 960 mJoule/cm^2 (or mJ/cm^2) [16]. Post-exposure, cells were subjected to cold shock at 4 or 10 °C for indicated times. The number of cells undergoing BCD or POD was counted by an inverted microscope (Olympus IX81 microscope with autofocus, Olympus, Tokyo, Japan). Also, time-lapse bright field and fluorescent microscopy (Nikon Eclipse TE2000-U, Tokyo, Japan) were carried out to image BCD or POD [16, 17]. Further, UV/cold shock-treated cells were imaged by time-lapse holographic microscopy (HoloMonitor M4, Phase Holographic Imaging PHI Inc., Boston, MA, USA) and analyzed by Hstudio M4 Tracking software.

Trypan blue exclusion test
Cells were stained with trypan blue to determine the extent of cell viability [16, 17]. Live cells exclude the trypan blue dye, whereas dead cells retain it. Cells in Petri dishes were washed with 1X phosphate-buffered saline (PBS) for one time and then incubated with 0.2% trypan blue in 1X PBS for 2 min. The dye was decanted, and the total cells and trypan blue-positive cells were counted.

MTT assay
MTT assay was used to measure functionally active metabolism in live cells [5, 14, 15]. Cells were seeded onto 96-well plates overnight, and then MTT was added for incubation at 37℃ for 4 h, then decanting the culture supernatants and adding 100 μL DMSO to dissolve the MTT-derived formazan purple crystals. Absorbance was measured using a SpectraMax M3 Multi-Mode Microplate Reader (Molecular Devices, San Jose, CA, USA) at a wavelength of 570 nm.

Chromosomal DNA fragmentation assay
Chromosomal DNA fragmentation assay was carried out [5, 14, 15]. Post UV/cold shock, cells were harvested and lysed with 50 μL lysis buffer (1% NP-40 in 20 mM EDTA, 50 mM Tris–HCl, and pH 7.5) for 10 s. These samples were centrifuged (1600 g, 5 min), and supernatants were harvested. This step was repeated once. The supernatants were added 1% SDS and RNase A (5 μg/μL) for incubation for 2 h at 56℃ and then treated with proteinase K (2.5 μg/μL) overnight at 37℃. After adding 1/2 volume of 10 M ammonium acetate, DNA preparations were precipitated with 2.5 volumes of ethanol, resuspended

in Milli-Q H_2O, and analyzed by 1.5% agarose gel electrophoresis.

Antibodies, co-immunoprecipitation, and Western blotting

Commercial antibodies used in this study were against: 1) lamin B1, 2) α-tubulin, 3) TRAF2, 4) WWOX (D-9), 5) Bclx, 6) Bak, 7) Bcl-2, 8) p53, 9) pS20-p53, 10) pS46-p53, 11) cortactin, 12) TRADD (the above antibodies from Santa Cruz Biotechnology, Santa Cruz, CA, USA), 13) β-actin (from Gentex), and 14) caspase 3 (from Promega). Homemade antibodies were against: 1) WWOX7-21, 2) pY33-WWOX, and 3) pS14-WWOX [15–17]. For Western blotting, cells were lysed with a lysis buffer (1% SDS, 0.5% NP-40, 0.1% Triton X-100) in the presence of 7 μL of a protease inhibitor cocktail (Sigma) plus 1 mM PMSF and 1 mM Na_3VO_4, and incubated on ice for 30 min. The lysates were centrifuged at 4℃ at 20,817 g (or relative centrifugal force) for 15 min (Eppendorf 5430/R microfuge) and then processed for standard SDS-PAGE and immunoblotting [15–19]. For co-immunoprecipitation [15–18, 31], 500 μg of the whole cell lysates (in 500 μL lysis buffer) were prepared and precleared with 23 μL protein G agarose beads (Invitrogen, Carlsbad, CA, USA) for 1 h. After centrifugation, the supernatants were harvested, and the pellets were discarded. A specific antibody (3 μg) or 4 μL homemade antiserum was added to the precleared lysate supernatants, followed by adding 18 μL protein agarose G beads and incubating in an end-over-end shaker for 6 to 18 h at 4℃. The beads were pelleted by centrifugation (8,990 g for 90 s) and washed four times. The antibody-bound proteins were released by adding an aliquot of reducing sample buffer and heating the beads at 90 °C for 10 min. Finally, SDS-PAGE, electrotransferring to nitrocellulose membranes, and Western blotting were carried out.

Immunofluorescence staining

Cells were cultured on coverslips overnight or 48 h. After the indicated experiments, cells were fixed with 3.7% paraformaldehyde for 20 min at room temperature and permeabilized with 0.5% Triton X-100 in 3.7% paraformaldehyde for another 10 min [15–18, 35]. Cells were washed three times with 1X PBS and added with 4% BSA for overnight incubation at 4 °C to block the nonspecific binding sites. For antigen detection, primary antibodies (in 4% BSA) were added to the cells for 2 h at room temperature, or 3 to 6 h at 4 °C. Cells were washed three times with 1X PBS and then stained for 1 h with fluorescent secondary antibodies, conjugated with red fluorescent rhodamine, Texas red, or Alexa 555 (Molecular Probes/Invitrogen, Eugene, OR, USA). For dual-color staining, secondary antibodies were conjugated with green fluorescent Alexa Fluor 488 or Fluorescein (Molecular Probes/Invitrogen) and counter-stained the nuclei with 4′,6-diamidino-2-phenylindole (DAPI) for 2 min. Confocal or immunofluorescence microscopy was then carried out.

Yeast two-hybrid analysis

The Ras rescue-based CytoTrap yeast two-hybrid analysis (Stratagene, La Jolla, CA, USA) was carried out to map the binding of WWOX with TRAF2 [14–17]. The procedure, which involves the binding of a cytosolic bait protein (e.g. pSos-WWOX) with a membrane-anchored target protein (pMyr-p53 or pMyr-TRAF2), triggers the Sos/Ras/Raf/MEK/ERK signal pathway, enabling the growth of mutant yeast *cdc25H* at 37 °C under a synthetic defined galactose media (−Ura, −Leu) in agarose plates. Without binding, no yeast growth occurred at 37 °C. Positive controls included WWOX/p53 physical association and MafB self-interaction, while empty pSos/pMyr vectors served as negative controls.

Quantification and statistics analysis

Where indicated, data were analyzed by one-way Anova and Student's *t* test using Microsoft Excel and Prism 7. Data were expressed as mean ± standard deviation. $p < 0.05$ was considered statistically significant.

Results

UV induction of BCD and POD, respectively, in WWOXf and WWOXd cells at room temperature and below

Six randomly selected WWOXf cell lines [16], including DU145, HCT116, $Wwox^{+/+}$ wild-type MEF, L929S, COS7, and Mv1Lu, were cultured overnight, exposed to UV irradiation (480 or 960 mJ/cm^2), and then subjected to time-lapse microscopy at room temperature (22 °C). The NO-dependent nuclear bubble formation, which is shown in each WWOXf cell line (see white stars), reveals in a time-dependent manner (Fig. 1A; Video S1; Fig. S1 for enlarged figures). Similarly, six randomly selected WWOXd cells, including MDA-MB-231, NB69, $Wwox^{-/-}$ knockout MEF, L929R, NIH-3T3, and 4T1, were subjected to UV exposure followed by time-lapse microscopy. WWOXd cells may undergo shrinkage and whole cell explosion due partly to the generated non-NO gas in the nuclei (Fig. 1B). Nuclear condensation occurred eventually. Typical morphological changes in L929R are shown in a video from time-lapse microscopy (Video S2). When L929S cells were exposed to UV irradiation (480 mJ/cm^2) and cold shock at 4 °C, the cells underwent time-related bubbling (see arrows for bubbles; Fig. 2A), suggesting that cold shock enhances BCD at 22 °C and below.
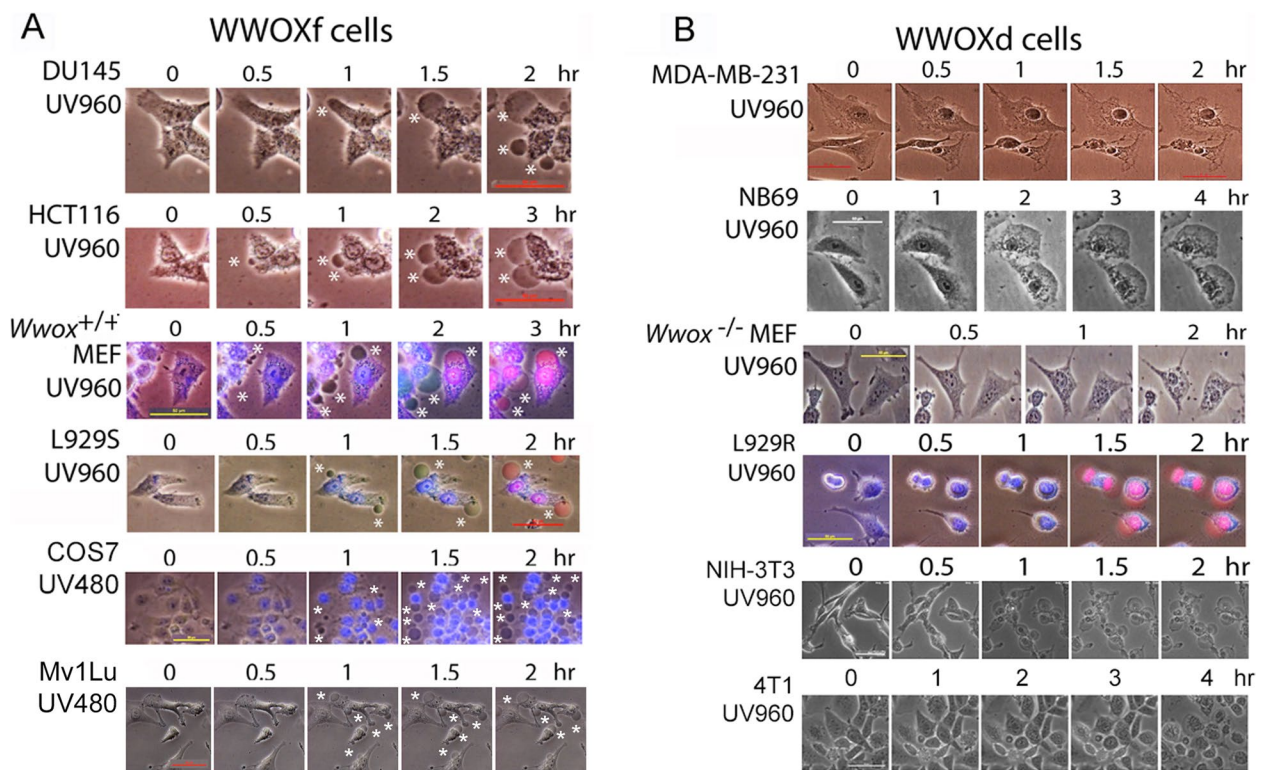
Fig. 1 UV induction of BCD in WWOXf cells and POD in WWOXd cells. **A** WWOXf cells, including DU145, HCT116, *Wwox*^{+/+} wild type MEF, COS7, Mv1Lu, and L929S cells, in 35-mm Petri dishes were exposed to UV (960 mJ/cm^2) and then subjected to time-lapse microscopy at 22 °C (200x; scale bar 50 μm). Bubbles were indicated by white stars. Also, see the enlarged figures in Fig. S1A. **B** Similarly, WWOXd cells, including MDA-MB-231, NB69, *Wwox*^{−/−} knock out MEF, 4T1, NIH-3T3, and L929R cells, were exposed to UV (960 mJ/cm^2), followed by time-lapse microscopy at room temperature (200x; scale bar 50 μm). Where indicated, cells were stained with nuclear stains DAPI (blue) and PI (red). Also, see the enlarged figures in Fig. S1B

Suppression of UV-mediated BCD by cold shock in WWOXf cells at 37 °C

We continued to examine the efficacy of BCD by stimulating WWOXf cells to UV only, UV then cold shock (4 °C for 5 min), or cold shock (4 °C for 5 min) then UV. Then, these cells were cultured at 4, 10, 22, and 37 °C, respectively, for indicated times (Fig. 2B-J). When MCF7 cells were treated with UV/cold shock or cold shock/UV, BCD occurred most effectively at 22 °C (Fig. 2B-D; Video S3). The BCD was blocked by greater than 70% at 37 °C, compared to other temperatures. For L929S cells, 4 °C was the best temperature for UV-mediated BCD (Fig. 2E-G). Cold shock blocked the UV-induced nuclear bubbling at 37 °C, compared to UV treatment only (Fig. 2E-G). Cold shock pretreatment inhibited unknown chemical reactions that strongly block BCD. Similarly, either UV/cold shock or cold shock/UV stimulated nuclear bubbling and BCD in COS7 cells at 4, 10, and 22 °C, but not at 37 °C (Fig. 2H-J). When COS7 cells were exposed to UV only, nuclear bubbling and BCD occurred at 4, 10, and 22 °C (Fig. 2H). The observations again suggest cold shock suppresses nuclear bubbling and BCD at 37 °C.

WWOXd L929R fibroblasts were exposed to UV only or UV and then cold shock. These cells underwent POD at 10 and 22 °C. However, POD was retarded at 37 °C under both conditions (Fig. 2K, L). In contrast, POD occurred in MDA-MB-231, MDA-MB-231(NH), and metastatic MDA-MB-231(IV-2–3) cells upon exposure to UV only or UV then cold shock (Fig. 2M-O). Temperature and treatment changes failed to alter the extent of POD (Fig. 2M-O and Video S4).

Reduction in cell viability during BCD

When COS7 cells were exposed to UV and incubated at room temperature for 2 h, the cells failed to exclude trypan blue (see red arrows; Fig. S2A). Similar results were observed in the UV/cold shock-treated COS7 cells (Fig. S2B). The observations indicate that the cells have reduced viability. Rapid loss of metabolic function occurred in UV-treated COS7 cells, as determined by MTT assay (Fig. S2C). Dramatically functional loss occurred if UV-irradiated cells were cultured overnight at 37 °C (Fig. S2D). COS7 cells were UV irradiated and cultured at 4, 22, or 37 °C for various durations. Subculture of these cells for overnight incubation at 37 °C
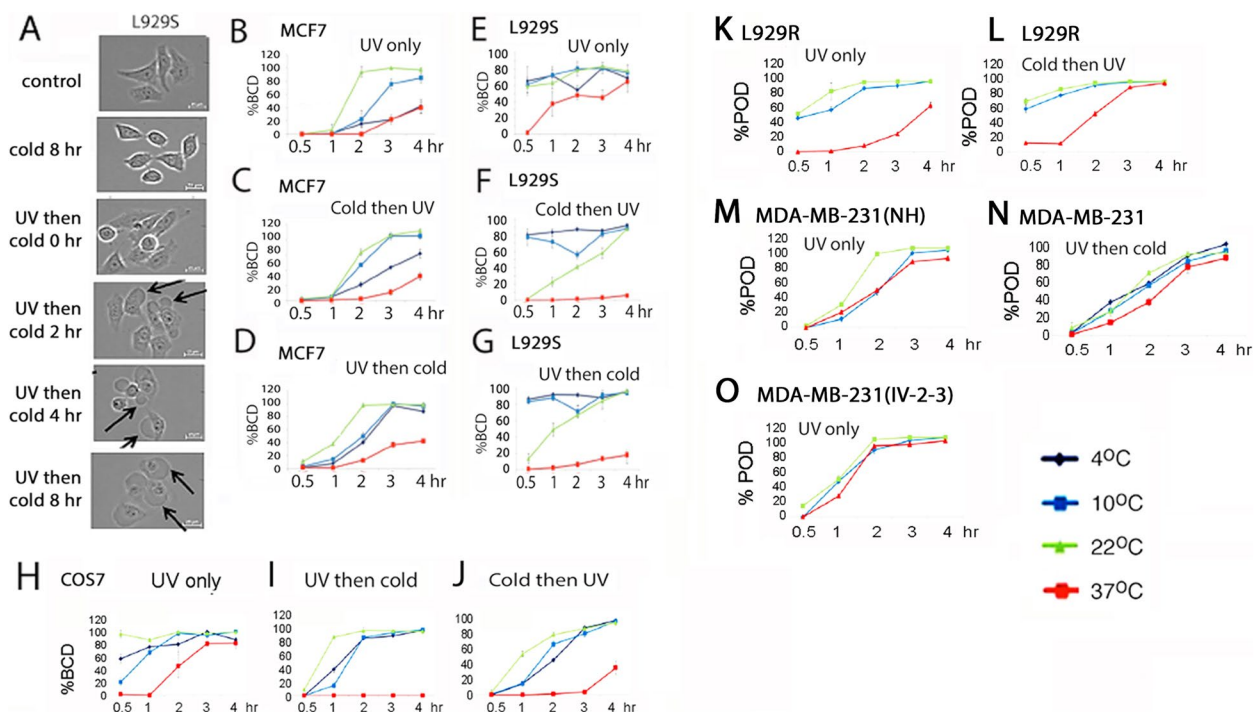
Fig. 2 UV/Cold shock-mediated BCD in WWOXf cell lines. **A** WWOXf L929S fibroblasts were exposed to UV (480 mJ/cm^2) and then cold shock at 4 °C for indicated times. Black arrows indicated bubbles. In controls, cells were treated with or without cold shock for 8 h. No bubble formation occurred. **B–D** WWOXf breast MCF7 cells were exposed to UV (480 mJ/cm^2) only (**B**), cold shock at 4 °C for 5 min and then UV (480 mJ/cm^2) (**C**), or UV (480 mJ/cm^2) and then cold shock at 4 °C for 5 min (**D**). The cells were then incubated at indicated temperatures for various durations, followed by measuring bubble formation (mean ± standard deviation; n = 3). **E-J** Similar results were observed when WWOXf L929S (**E–G**) and COS7 (**H-J**) cells were subjected to identical treatments. **K, L** WWOXd L929R were treated with UV only or cold shock then UV. The cells exhibited similar profiles in POD. The efficiency of POD was retarded at 37 °C. **M–O**, Two identical MDA-MB-231 cell lines (original and NH) and a metastatic line (IV-2–3) were treated similarly with UV and/or cold shock under different temperatures. The POD profiles were very similar despite the changing temperatures and various UV and/or cold shock treatments

resulted in cell death by > 90% (Fig. S2E). Similar results were observed when these UV-treated cells were cultured overnight at 37 °C (Fig. S2F). Rapid suppression of metabolic function was observed when the UV-treated COS7 cells were cultured at 4 °C for 1–4 h, compared to other temperatures (Fig. S2G).

Failure of mitochondrial apoptosis-inducing chemicals in blocking BCD

Next, COS7 cells were treated with betulinic acid (10 μM) or staurosporine (1 μM) for 1 h to initiate mitochondrial apoptosis, and then exposed to UV and cold shock (4 °C for 5 min), followed by incubation at room temperature for indicated times. Compared to UV/cold shock-treated cells, pre-induction of mitochondrial apoptosis did not block BCD (Fig. S2H). When COS7 cells were pretreated with caspase inhibitor I or caspase inhibitor X, these cells still underwent BCD (Fig. S2H).

Internucleosomal DNA fragmentation was not detected in the UV/cold shock-treated cells during incubation at 22 °C (Fig. S2I). When L929S, but not COS7, were exposed to UV and then cultured at 37 °C for 8 h, DNA fragmentation occurred (Fig. S2J, K). As positive controls, staurosporine at 1 μM induced DNA fragmentation at 37 °C but not at 22 or 4 °C (Fig. S2J, K). Failure of UV-treated COS7 cells to undergo DNA fragmentation during incubation for 8 h at 37 °C was probably due to insufficient incubation time.

Necroptosis inhibitors incapable of blocking UV/cold shock-induced BCD in WWOXf cells and POD in WWOXd cells

When L929S cells were pretreated with a necroptosis inhibitor Nec-1 or GSK'872 for 1 h, and then exposed to UV (480 mJ/cm^2) and cold shock for 5 min at 4° C, the treated cells exhibited bubbling in 1.5 h (Fig. S3A). Compared to controls, no retardation was observed. Similarly, pretreatment of L929S cells with necroptosis inhibitors Nec-1 for 30 min failed to abolish the nuclear bubbling (Fig. S3A). Under similar conditions, L929R cells underwent UV-mediated POD, and Nec-1 failed to block the

Chen *et al. Cell Communication and Signaling*   (2024) 22:505

Page 7 of 16

effect (Fig. S3B). The observations suggest that necroptosis is not involved in BCD or POD.

Suppression of BCD in WWOXf cells by antioxidant U74389G at 22 °C

To further elucidate the mechanisms underlying nuclear bubbling, WWOXf SCC15 cells were pretreated with EGTA (1 mM), proteasome inhibitor MG132 (30 μM) [36, 37], p53 activator Prima-1 (30 μM) [38–40], CHK2/ATM inhibitor (30 μM) [41, 42], or antioxidant U74389G (30 μM) [43–45] for 30 min. These cells were then exposed to UV irradiation (480 mJ/cm^2) or UV/cold shock (5 min at 4 °C). By time-lapse microscopy at room temperature, U74389G strongly suppressed the nuclear bubbling (Fig. S4). EGTA, a calcium ion chelator, also retarded the occurrence of BCD (Fig. S4). No inhibitory effects were observed for MG132 and Prima 1, whereas CHK2/ATM inhibitor enhanced the occurrence of BCD.

UV or UV/cold shock induction of NO production and calcium influx in WWOXf cells but not in WWOXd cells

We investigated the role of calcium (Ca^{2+}) influx and NO production for nuclear bubbling in UV or UV/cold shock-induced BCD. WWOXf HCT116 cells were exposed to UV (960 mJ/cm^2) and then cold shock at 4 °C for 10 min. Endogenous NO production was then measured by using a live cell dye, DAF-FM [46], for time-lapse microscopy at 22 °C (Fig. 3A, B). The nuclear bubbling (see red arrows) occurred 30 min after NO production, suggesting that the increased NO is responsible for nuclear bubbling. Under similar conditions, UV/cold shock could not effectively raise the levels of intracellular NO in WWOXd 4T1 cells (Fig. 3C).

When HCT116 cells were pretreated with a calcium chelator EGTA at 200 μM for 1 h at 37 °C, calcium influx was retarded in 30 min, as measured by a live cell stain Fluo-8 (Fig. 3D). The first bubbling at 22 min was
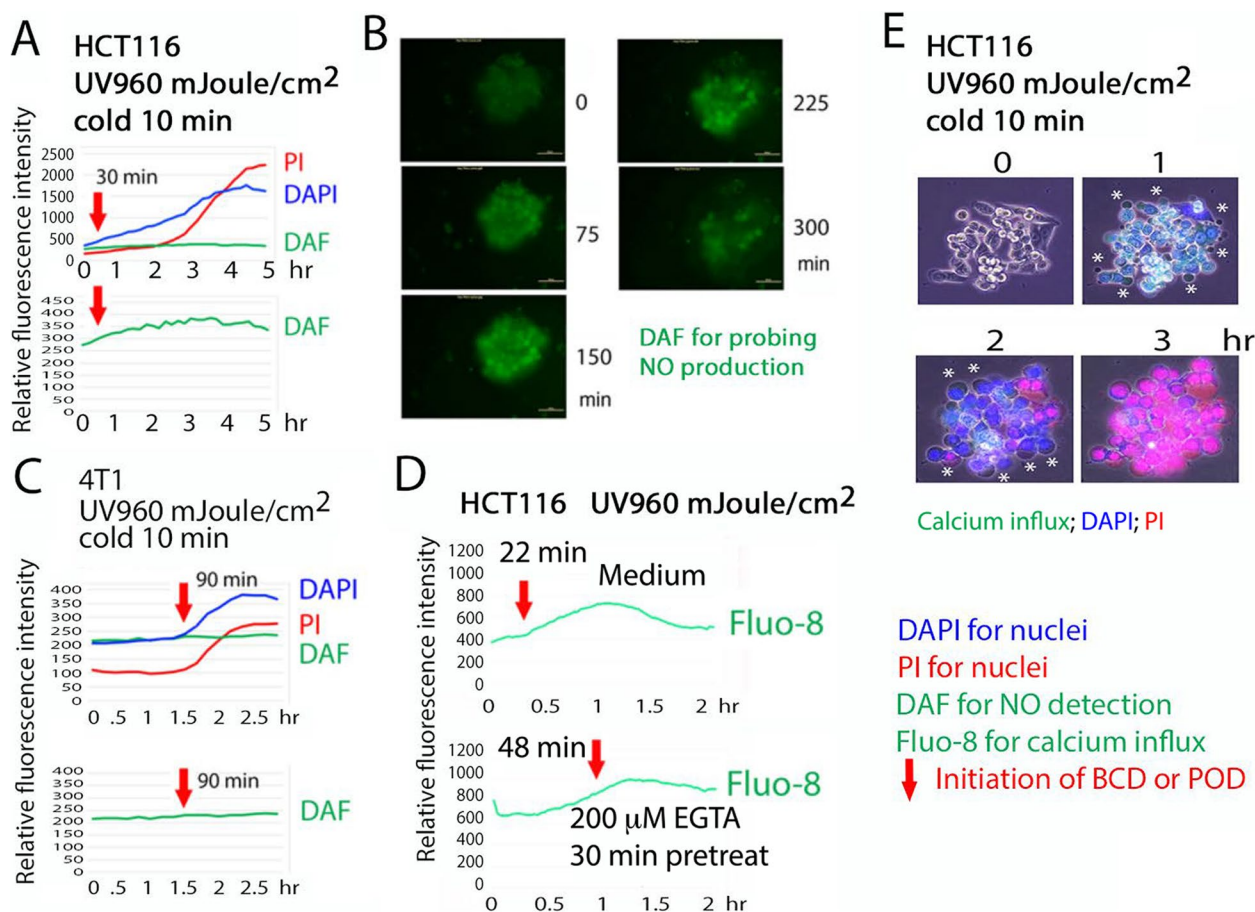

Fig. 3 Calcium influx and NO production during UV/cold shock-mediated nuclear bubbling. **A, B** WWOXf HCT116 cells were exposed to UV and then cold shock at 4 °C for 10 min. Increased NO production was shown (stained with green fluorescent DAF). Red arrows indicate the time of initiation of nuclear bubble formation. **C** Under similar conditions, WWOXd 4T1 cells had little or no increased production of NO. **D** Calcium influx was observed in UV-treated HCT116 cells (stained with green fluorescent Fluo-8). Calcium chelator EGTA retarded the bubble formation. **E** HCT116 cells were added 1 μL of DAF for probing Ca^{2+} ion (green) and DAPI (blue) and PI (red) for staining nuclei, followed by exposure to UV (960 mJ/cm^2) and cold shock at 4 °C for 10 min, and then time-lapse microscopy at 22 °C

Chen *et al. Cell Communication and Signaling*   (2024) 22:505

Page 8 of 16

prolonged to approximately 48 min at 22 °C (Fig. 3D). To be effective, greater than 1 mM EGTA was needed to achieve 50% inhibition of calcium influx at 22 °C. These observations suggest that NO production and calcium influx co-occur and calcium ions support the formation of nuclear bubbles. The NO bubbles shrink and disappear quickly without sufficient calcium ions in the microenvironment. A summary panel of images shows the time-related event of UV/cold shock-treated HCT116 cells, involving initial calcium influx (green), DAPI uptake, and final PI uptake in the nuclei (Fig. 3E).

Dramatic increases in cell thickness during apoptosis and division but not BCD, as determined by time-lapse holographic microscopy

Next, we investigated cell morphological changes during BCD by time-lapse holographic microscopy [47]. The imaging technique allows visualization of three-dimensional changes of cell division, apoptosis, and BCD. Cell bubbling occurred when WWOXf COS7

cells were exposed to UV and cold shock at various durations at 4 °C (Fig. 4A; magnification at $100\times$ and $400\times$ for Videos S5 and S6, respectively). The thickness of cell bubbles was significantly shorter than the body of L929S cells (shorter than 2 to 3 μm; Fig. 4B, C; Video S7). When L929S cells were treated with staurosporine and cultured at 37 °C, the cells underwent apoptosis, which showed whole cell shrinkage and increased thickness, reaching ~12 μm (Fig. 4D; Video S8). In comparison, apoptosis occurred when UV/cold shock-treated L929S cells were cultured at 37 °C, and the cell thickness reached ~15 μm (Video S9). No bubble formation was observed. During cell division, L929S cells started getting tall (~17 μm) and then underwent division (Video S10). During BCD, there were brief increases in cell volumes followed by reduction, and cell areas remained relatively stable (Fig. 4E). When cells underwent apoptosis, cell areas and volumes were reduced. However, cells became taller, lasting 5–8 h (Fig. 4E). These observations clearly show the
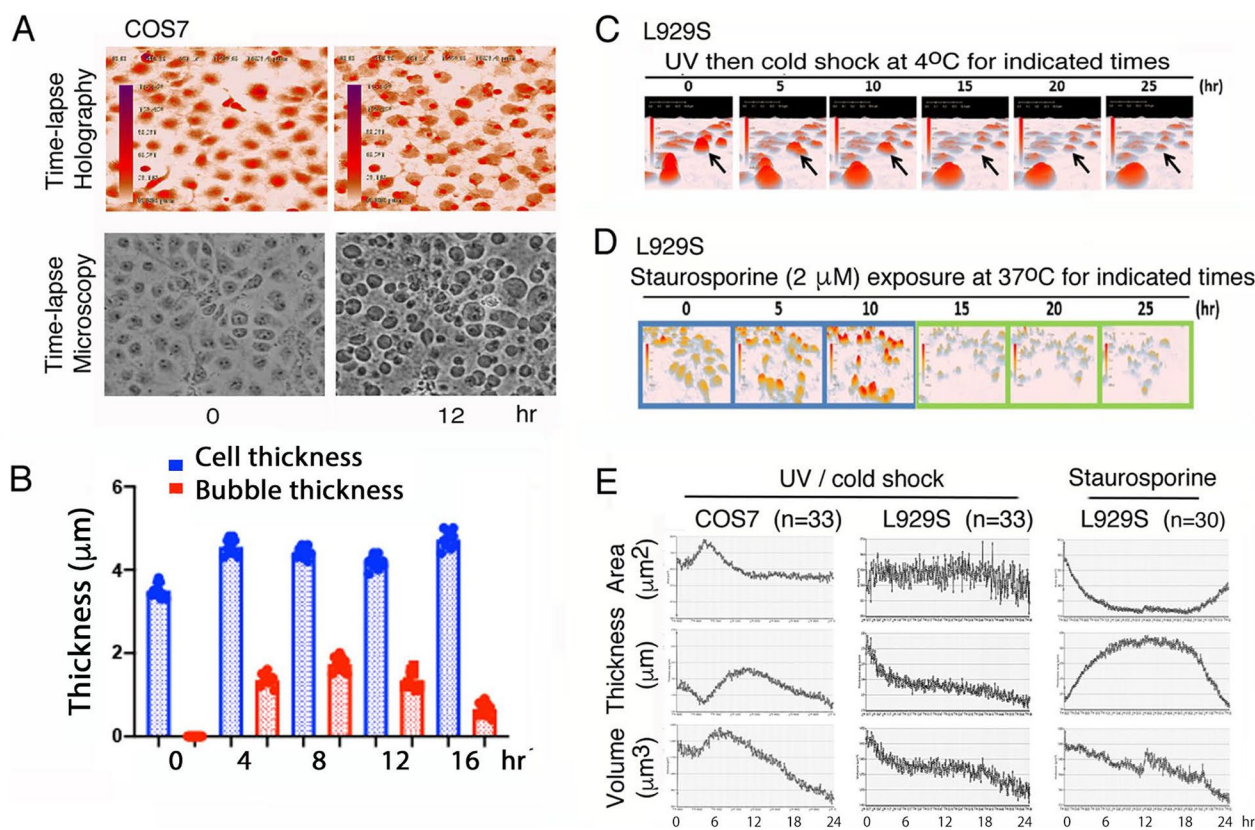

Fig. 4 Dramatic increases in cell thickness during apoptosis, but not BCD, determined by time-lapse holographic microscopy. **A**, **B** COS7 cells were exposed to UV and then cold shock at 4 °C for 12 h. Cell bubbles were observed, as determined by light and holographic microscopy, respectively. The COS7 cell thickness (height) is approximately 4.5 μm, and the bubble thickness less than 2 μm ($n = 10$; $p < 0.0001$ versus time zero controls; Student's t-test). **C** Under similar conditions, time-related bubbling is shown at 4 °C in L929S cells. **D** By contrast, staurosporine-induced apoptosis of L929S cells at 37 °C exhibited condensation and increased whole cell thickness reaching ~12 μm. **E** A summarized graph shows the changes in area, thickness, and volume of COS7 and L929S cells during BCD and apoptosis

Chen *et al. Cell Communication and Signaling*   (2024) 22:505

Page 9 of 16

fundamental differences between BCD and apoptosis, especially in the cell heights.

UV/cold shock or UV-mediated downregulation of caspase 3, Bak, and α-tubulin

We examined whether UV/cold shock affects protein expression in cells. COS7 cells were exposed to UV irradiation and incubated at 4℃ for indicated times. Downregulation of house-keeping proteins α-tubulin and β-actin occurred rapidly (Fig. 5A; > 70% for α-tubulin and > 30% for β-actin). Cortactin, a protein involved in cell shape and migration [48], was downregulated rapidly in UV-irradiated COS7 cells (Fig. 5A; > 90%). In response to UV/cold shock, the level of p53 was relatively
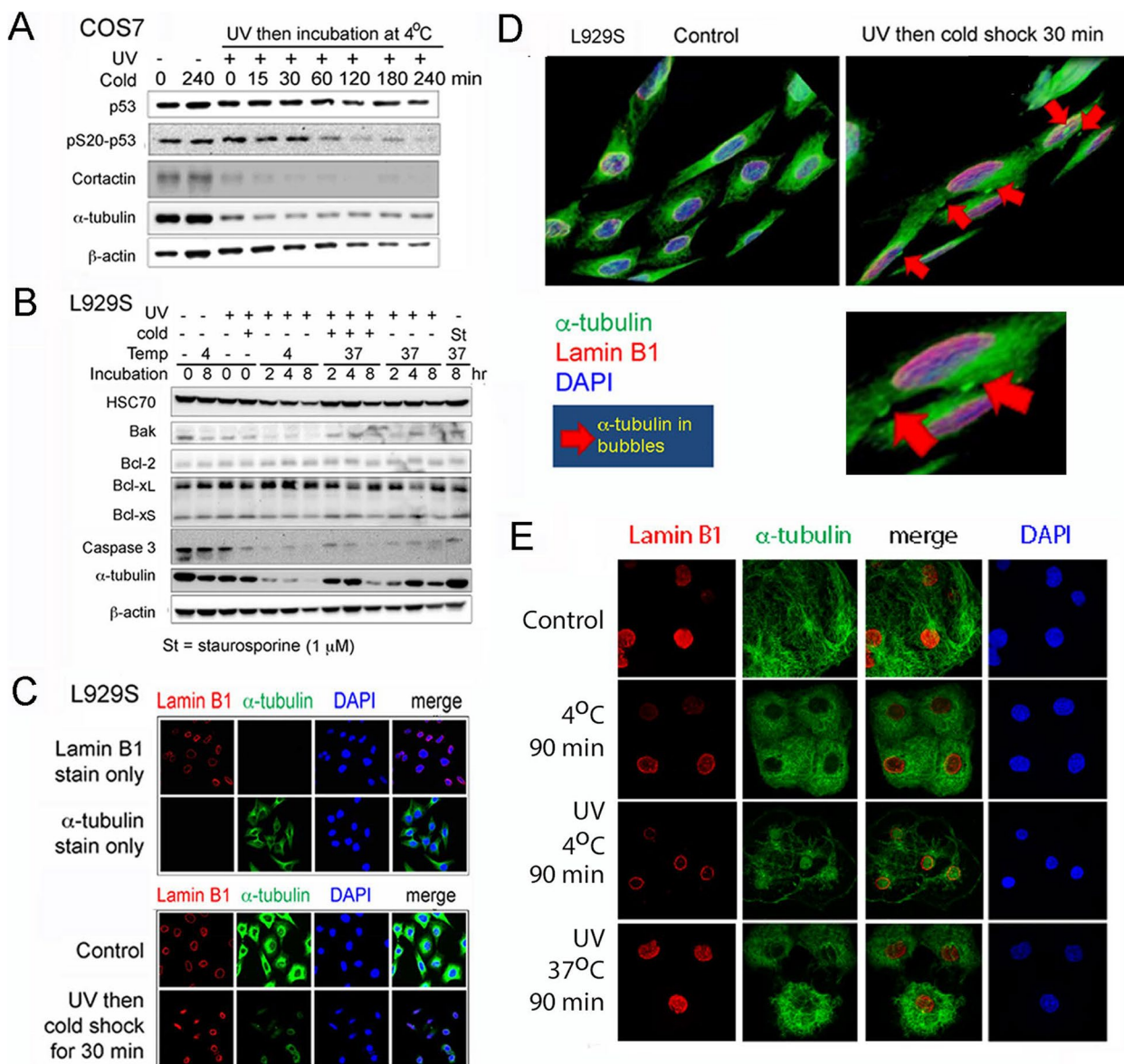

Fig. 5 Downregulation of housekeeping proteins and leaking of cytosolic α-tubulin to the enlarging nuclear bubbles during BCD. **A** COS7 cells were UV irradiated (480 mJ/cm²) and cold shocked for indicated times, which led to rapid downregulation of cortactin and α-tubulin. **B** L929S cells were exposed to UV (480 mJ/cm²) and then cold shock for 5 min and incubated at 4 or 37 °C for indicated times. UV/cold shock downregulated caspase 3, Bak, and α-tubulin at 4 °C. **C, D** L929S cells were treated with or without UV/cold shock. Confocal microscopy shows downregulation of α-tubulin (bottom panel; magnification: 1000X) (**C**). α-Tubulin was shown in the bubbles (right panel; red arrows) (**D**). **E** COS7 cells were treated with UV (480 mJ/cm²) and then cultured at 4 or 37℃ for 90 min, or 4 °C for 90 min without UV exposure. When cells were treated with UV/cold shock, α-tubulin was downregulated and depolymerized during continuous culture at 4 °C. At 37℃, the cells underwent apoptosis (confocal microscopy; magnification: 1000X). The filamentary structure of α-tubulin was remodeled. Lamin B1 is a nuclear membrane protein

unchanged (< 20% reduction), whereas reduced p53 phosphorylation at S20 occurred in a time-related manner (Fig. 5A; > 90% reduction in 2 h).

Under similar conditions, L929S cells were exposed to UV and then cold shock, followed by incubation at specified temperatures for indicated times (Fig. 5B). UV/cold shock or UV alone drastically downregulated the expression of caspase 3, Bak and α-tubulin by greater than 90% in L929S cells at 4 °C (Fig. 5B). Bcl-2, Bcl-x (Bcl-xL and Bcl-xS) and heat shock protein 70 (HSC70) were less affected (< 10%; Fig. 5B). The reduction of caspase 3 may account for the failure of BCD-induced internucleosomal DNA fragmentation at room temperature or 4 °C (Fig. 5B). UV/cold shock-treated cells failed to migrate due, in part, to drastic loss of α-tubulin and cortactin.

UV/cold shock-mediated relocation of α-tubulin to the nucleus and nuclear bubble

By confocal microscopy, lamin B1 was shown to localize in the nuclear membrane and α-tubulin in the cytoplasm of untreated L929S cells (Fig. 5C). When L929S cells were exposed to UV and cold shock, downregulation of α-tubulin and nuclear condensation occurred (Fig. 5C). Merge of confocal sections for nucleus (DAPI), lamin B1 and α-tubulin is shown (Fig. 5D). UV/cold shock-treated L929S cells exhibited relocation of α-tubulin to the nuclear bubble (Fig. 5D, right panel; red arrows; also see an enlarged insert). The inner membrane of the bubble is from the nucleus, and the outer membrane is from the cell membrane [13, 14]. Accumulating evidence shows that α-tubulin is associated with apoptosis [49, 50].

Next, we examined whether α-tubulin undergoes morphological changes caused by UV/cold shock exposure. COS7 cells were exposed to UV (480 mJ/cm^2) and then cultured at 4 or 37℃ for 90 min. UV rapidly decreased the expression of α-tubulin, whereas cold shock had no effect (Fig. 5E). Compared to control cells (Fig. 5E), cold shock shrank the cells and reduced the cell sizes (Fig. 5E). In contrast, UV/cold shock-treated cells, which underwent BCD, had reduced levels of α-tubulin and the α-tubulin appears to be depolymerized (Fig. 5E). Notably, presence of the α-tubulin in the nucleus was observed (Fig. 5E). At 37℃, UV-treated cells underwent apoptosis, and α-tubulin did not relocate to the nuclei (Fig. 5E).

UV/cold shock induction of nuclear accumulation of TRAF2/WWOX complex to regulate bubbling

We further elucidated the functional interactions between TRAF2 and WWOX during BCD. When L929S cells were exposed to UV (480 mJ/cm^2) and then cold shock at 4℃ for 15 min to 4 h, expression of WWOX, TRAF2, and α-tubulin was downregulated by greater than 50% (Fig. 6A). Cold shock alone did not affect the expression of WWOX, TRAF2 and α-tubulin (Fig. 6A). pY33-WWOX levels were not reduced. Cold shock or UV/cold shock gradually reduced p53 expression (Fig. 6A).

Next, we investigated the functional role of TRAF2 domains in regulating BCD. A schematic graph for the primary structure of TRAF2 is shown (Fig. 6B). We reported the inhibition of UV/cold shock-mediated BCD in COS7 cells by transiently overexpressing TRAF2(113–312) of the zinc finger domain and the full-length of TRAF2 (14). An EGFP-TRAF2(124–233) construct was made for transient expression of the zinc finger domain in TRAF2. We established stable transfectants of L929S cells expressing EGFP-TRAF2(124–233), ECFP-TRAF2, ECFP, or EGFP (Fig. 6B). EGFP-TRAF2(124–233) strongly suppressed UV/cold shock-induced BCD. The full-length ECFP-TRAF2 was not expressed properly in this experiment and did not exhibit an inhibitory activity (Fig. 6B). Similarly, when COS7 cells were stably transfected with EGFP-TRAF2(124–233), suppression of BCD was observed Fig. 6C). Also, the full-length ECFP-TRAF2 inhibited BCD in L929S cells in a time-related manner (Fig. 6D; $p < 0.05$ for ECFP versus ECFP-TRAF2 in each time point; Student's t test).

By Cytotrap yeast two-hybrid analysis [6, 14–17], we determined the positive binding of full-length WWOX with full-length TRAF2 to allow mutant yeast growth at 37 °C (Fig. 6E). In positive controls, p53 physically bound WWOX and MafB underwent self-association (Fig. 6E). In negative controls, empty pSos and pMyr did not support yeast growth at 37 °C. TRAF2 did not bind the SDR domain of WWOX (Fig. 6E), suggesting that the *N*-terminal WW domains of WWOX interact with TRAF2. Additionally, we carried out Förster resonance energy transfer (FRET) microscopy [14–17]. There was an increased binding of EGFP-TRAF2 with DsRedM (monomeric DsRed)-WWOX in UV/cold shock-treated COS7 cells at 37 °C (Fig. 6F). At a low temperature (4 °C), the EGFP-TRAF2/DsRedM-WWOX complex became dissociated in 60 min (Fig. 6F).

Co-relocation of TRAF2 and WWOX complex to the nucleus in response to UV/cold shock

By fluorescent immunostaining, UV/cold shock-induced nuclear co-localization of endogenous WWOX with TRAF2 occurred in COS7 cells (Fig. 7A). In the absence of WWOX, endogenous TRAF2 in *Wwox*$^{-/-}$ knockout MEF cells did not undergo UV/cold shock-mediated relocation to the nucleus (Fig. 7B), suggesting that TRAF2 requires WWOX to co-translocate to the nucleus. In
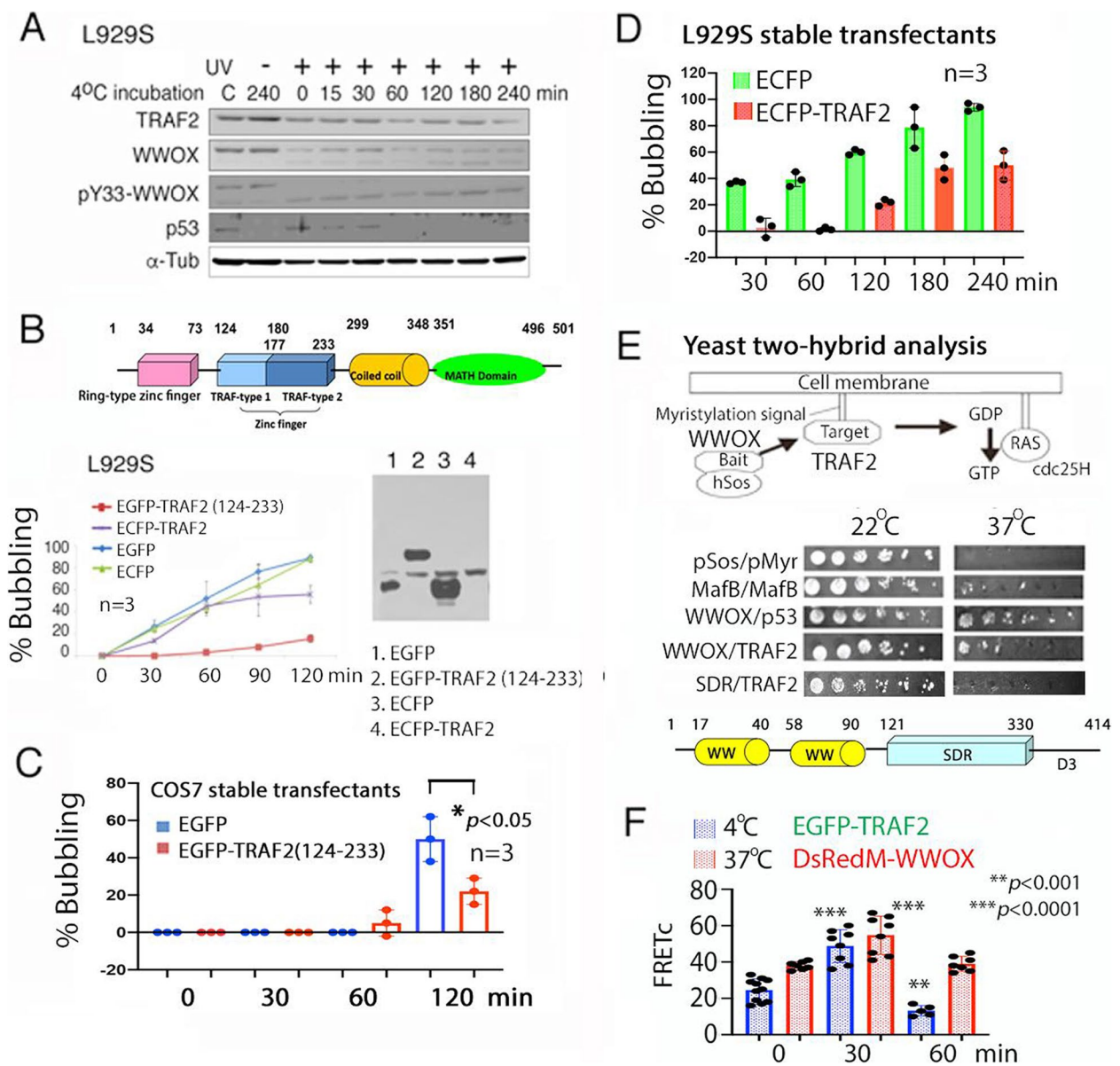
Fig. 6 Dissociation of TRAF2/WWOX complex at low temperature leading to BCD suppression. **A** L929S cells were exposed to UV (480 mJ/cm²) and then cold shock at 4°C for indicated times. UV/cold shock downregulated WWOX, TRAF2 and α-Tubulin proteins by ∼ 50%. The cold shock alone had no apparent effect. **B** The primary structure of TRAF2 is shown. The L929S cell stable transfectant, expressing EGFP-TRAF2(124–233), strongly resisted UV/cold shock-induced BCD. The full-length ECFP-TRAF2 was not expressed and did not inhibit BCD. **C**, **D** Ectopic EGFP-TRAF2(124–233) and ECFP-TRAF2 blocked BCD in COS7 and L929S stable transfectants, respectively. **E** Cytotrap yeast two-hybrid analysis showed the binding of WWOX with TRAF2. p53/WWOX and MafB/MafB complexes are positive controls. **F** FRET microscopy revealed the increased binding of EGFP-TRAF2 with DsRedM-WWOX in UV/cold shock-treated COS7 cells at 37 °C, whereas the binding was significantly reduced at 4 °C during incubation for 60 min

the knockout $Wwox^{-/-}$ MEF cells, UV/cold shock did not cause the translocation of cytosolic TRAF2 to the nucleus in (Fig. 7C). However, p53 localized in both cytoplasm and nucleus (Fig. 7C).

Occurrence of the TRAF2/WWOX complex dissociation and increased p53/WWOX complex formation at low temperatures

By co-immunoprecipitation, UV/cold shock induced the dissociation of the endogenous WWOX/TRAF2 complex in 30 min in COS7 cells (Fig. 7D). TRADD, a
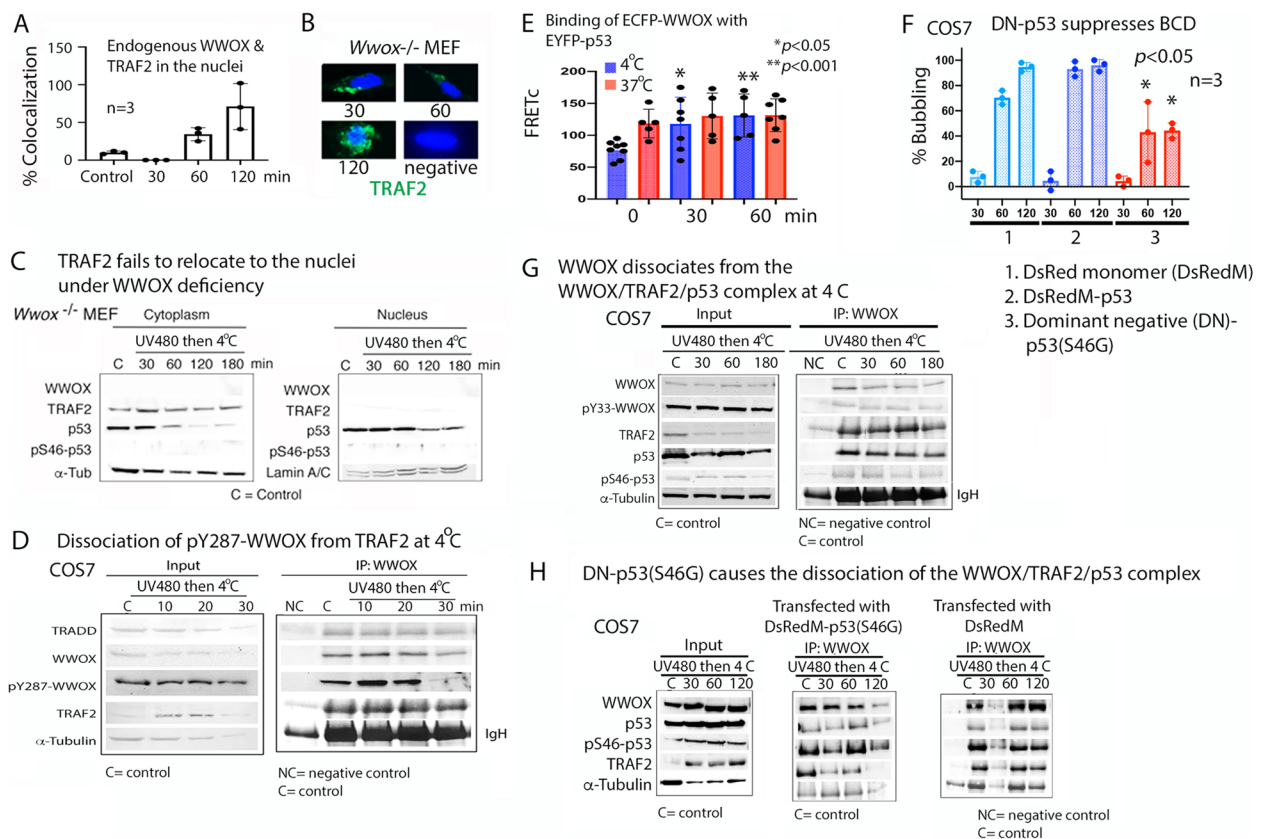
Fig. 7 Co-translocation of WWOX with TRAF2 to form complex with p53 in the nucleus. **A** Endogenous WWOX co-translocated with TRAF2 to the nuclei in COS7 cells by UV (480 mJ/cm^2) and cold shock at 4 ℃ in a time-dependent manner. **B** Endogenous TRAF2 (stained in green) in *Wwox*$^{-/-}$ knockout MEF cells did not relocate to the nuclei (stained with DAPI) in response to UV/cold shock (~ 200 cells counted). **C** UV/cold shock did not induce translocation of cytosolic TRAF2 to the nucleus in *Wwox*$^{-/-}$ MEF cells. **D** UV/cold shock induced the dissociation of pY287-WWOX from the WWOX/TRAF2/TRADD complex in 30 min in COS7 cells, as determined by co-immunoprecipitation. **E** FRET microscopy revealed the increased binding of EYFP-p53 with ECFP-WWOX at 4℃. **F** Dominant negative (DN)-p53 significantly blocked UV/cold shock-mediated BCD. **G** Co-immunoprecipitation revealed that WWOX dissociated from the endogenous p53/TRAF2 complex in UV/cold shock-treated COS7 cells. **H** Transiently overexpressed DN-p53(S46G) caused WWOX dissociation from the endogenous TRAF2/WWOX/p53 complex at 4℃. In controls, ectopic monomeric DsRedM had no effect

TNF receptor adaptor protein [51], physically bound TRAF2 without dissociation during UV/cold shock (Fig. 7D). Dissociation of the TRAF2/WWOX complex correlates with WWOX dephosphorylation at Y287. pY287-WWOX is subjected to ubiquitination and proteasomal degradation [44]. Notably, there was an increased complex formation for p53 and WWOX at 4°C, as determined by FRET microscopy (Fig. 7E). Accordingly, transiently overexpressed dominant negative (DN)-p53(S46G) abolished UV/cold shock-mediated BCD (Fig. 7F). pS46-p53 is known to bind pY33-WWOX in UV-treated cell lines [37]. p53 was cloned in a pDsRed monomer (pDsRedM) vector to prevent the self-binding of p53 when expressed in cells. In controls, DsRedM-p53 and DsRedM were not able to block BCD (Fig. 7F). We confirmed the observations by co-immunoprecipitation that WWOX became dissociated from the WWOX/TRAF2/p53 complex in UV/cold shock-treated COS7 cells (Fig. 7G). The complex exhibited the presence of pY33-WWOX and pS46-p53 when interacting with TRAF2. Again, by co-immunoprecipitation, transiently overexpressed DN-p53(S46G) caused the dissociation of TRAF2 from the WWOX/TRAF2/p53 complex in COS7 cells at 4°C (Fig. 7H).

Together, in response to UV/cold shock, WWOX binds and carries TRAF2 to relocate to the nucleus, followed by dissociation at 4°C. The zinc finger domain of TRAF2 blocked the function of WWOX/p53 in inducing BCD at low temperatures. Conceivably, dissociation of the complex at low temperatures facilitates the function of WWOX, p53, NOS2 (nitric oxide synthase) and other related proteins to induce NO production [13, 14].

Chen *et al. Cell Communication and Signaling*   (2024) 22:505

Page 13 of 16

Discussion

This study concerns UV/cold shock-mediated frostbite in humans and animals. The disaster may accidentally occur in the polar regions or outer space. In particular, increased human travel to the outer space is expected in the near future. If an accident occurs during the travel, humans will get exposed to strong ultraviolet irradiation such as UVC (wavelength 100 to 280 nm) and extreme cold and die immediately [52]. Here, we first demonstrate the presence of a temperature-sensitive WWOX/TRAF2/p53 complex for regulating UV-mediated cell death. We determined that UV induces WWOXf cells to undergo BCD and WWOXd cells to undergo POD at low temperatures (less than 22 ℃). Reduced cell viability occurs during BCD. BCD cannot be effectively blocked by chemicals in modulating mitochondrial apoptosis such as staurosporine, betulinic acid, and caspase inhibitors. Inhibitors of necroptosis Nec-1 and GSK'872 fail to block UV/cold shock-induced BCD in WWOXf cells and POD in WWOXd cells. Significantly, antioxidant U74389G strongly suppresses BCD in WWOXf cells at 22 ℃. The observation agrees with our previous report that NO production is needed for BCD [13, 14]. UV or UV/cold shock induces simultaneous NO production and calcium influx in WWOXf cells. However, neither event occurs in the UV or UV/cold shock-treated WWOXd cells. In WWOXf cells, dramatic increases in cell thickness or height occur during apoptosis, but not BCD, as determined by time-lapse holographic microscopy. Whether this event happens in WWOXd cells is unknown. UV/cold shock or UV alone downregulates caspase 3, Bak, cortactin, and α-tubulin, and induces relocation of α-tubulin to the nucleus and the nuclear bubble. Downregulation of cortactin and cytoskeletal proteins renders immobility in cells.

We determined that the cell morphological changes during BCD and POD are unique, unlike in apoptosis or necrosis [11, 12]. Furthermore, BCD, unlike apoptosis, is an irreversible cell death event [13, 14]. A fascinating aspect is the role of cold shock in enhancing the UV-mediated NOS2 accumulation in the nucleus for NO production and bubble formation [13, 14]. This event, distinct from apoptosis or necrosis, is a testament to the complexity of cellular processes. Notably, the NO levels are barely detectable in the WWOXd cells, and UV fails to increase nuclear NO production. These intriguing observations suggest that WWOX works together with NOS2 to induce NO production. The use of nω-nitro-L-arginine methyl ester hydrochloride (Nω-LAME), an inhibitor of NO synthase, has revealed that it blocks NO production in WWOXf cells [14]. UV, on the other hand, increases cell membrane permeability, allowing rapid DAPI accumulation in the cytoplasm. As the nuclear bubble enlarges to a certain extent, PI uptake in the nuclei occurs. This is due to the increased permeability of nuclear membrane and the enlarged nuclear pores [14].

Our study has uncovered a crucial finding: the dramatic downregulation of antiapoptotic TRAF2 during frostbite in human skin [13, 14]. This discovery, along with the revelation that TRAF2 counteracts the function of WWOX and p53 in inducing BCD, not only enhances our understanding of molecular biology but also has practical implications. In response to UV only or UV/cold shock, WWOX binds TRAF2 to co-translocate to the nucleus in WWOXf cells. No nuclear translocation for TRAF2 occurs in *Wwox* knockout MEF cells, suggesting that WWOX carries TRAF2 to migrate to the nucleus. At low temperatures (22 ℃ and below), WWOX preferentially dissociates itself from interacting with TRAF2 in the nucleus. WWOX gains a tighter binding with p53 to carry out BCD at low temperatures. Proapoptotic tumor suppressors WWOX and p53 are known partners in causing apoptosis and BCD [6, 13, 14, 53–56].

We determined that the zinc finger domain of TRAF2 blocks the function of WWOX/p53 in inducing BCD at low temperatures. The binding of the zinc finger domain of TRAF2 with the Y33-phosphorylated first WW domain of WWOX is suggested. At 37 ℃, the WWOX/TRAF2/p53 is intact and stable, facilitating apoptosis. Cells undergo BCD at low temperatures. BCD stops when the surrounding temperature is raised to 37 ℃, and apoptosis resumes. Again, the TRAF2/WWOX complex dissociates at low temperatures, and p53/WWOX complex formation is increased to push BCD forward. Accordingly, WWOX/TRAF2/p53 is a temperature-sensitive molecular switch controlling the transition between BCD and apoptosis—treatment of localized skin cancer with liquid nitrogen results in downregulating TRAF2 but upregulating WWOX [14]. The proapoptotic WWOX causes skin cancer cell death, suggesting a potential new approach for cancer treatment..

By FRET analysis, we showed the binding of EGFP-TRAF2 with DsRedM-WWOX, and the complex becomes readily dissociated at 4 ℃. However, the complex is relatively stable at 37 ℃. WWOX is tagged with a monomeric DsRed, which may make it easily dissociated from TRAF2. By co-immunoprecipitation, we determined the presence of the TRADD/TRAF2/WWOX/p53 complex. This complex is relatively stable. However, when WWOX is Y287 phosphorylated, pY287-WWOX becomes dissociated from the complex. Whether pY287-WWOX is subjected to ubiquitination and proteasomal degradation remains to be established. Our recent studies determined that the stronger the binding of WWOX with intracellular protein partners, the weaker the cancer cells grow [57–59]. Thus, a scenario is that when

pY287-WWOX is dissociated from the TRADD/TRAF2/ WWOX/p53 complex, the UV/cold shock-treated cells are readily subjected to death. UV induces p53 and WWOX to undergo nuclear translocation [53–55]. Trafficking protein TRAPPC6A carries WWOX to relocate to the nucleus [2, 60]. TRAPPC6A can be a tour guide for leading the TRADD/TRAF2/WWOX/p53 complex to undergo nuclear translocation.

When the ambient temperature goes up from 22 °C to 37 °C, BCD readily stops and switches to apoptosis [13, 14]. Similarly, ongoing apoptosis turns into BCD when the temperature drops from 37 °C to 22 °C and below [13, 14]. Unlike apoptosis, no internucleosomal DNA fragmentation occurs during BCD. When L929S cells are exposed to UV, downregulation of caspase 3 occurs. This downregulation may account for the failure of internucleosomal DNA fragmentation during BCD at room temperature and below. EGTA, at 1 mM, retards the formation of a nuclear bubble, suggesting that calcium ion is needed for bubble formation. When cells are exposed to greater than 2 mM EGTA, bubble formation is disrupted, suggesting that calcium ion strengthens the bubble membrane stability.

Supporting evidence showed that caspase 1 and reactive oxygens participate in BCD as lazaroid antioxidant U74389G strongly retards nuclear bubble formation by greater that 15 h. Inhibition of proteasomes by MG132 does not block BCD. Activation of p53 by Prima-1 slightly retards nuclear bubbling. Inhibition of checkpoint kinases by CHK2/ATM inhibitor does not affect nuclear bubble formation. Inhibitors of necroptosis such as Nec-1 and GSK'872 cannot block UV/cold shock-induced nuclear bubbling in L929S cells. Similarly, Nec-1 does not inhibit UV/cold shock-induced nuclear explosion in L929R cells.

Hypothetically, the jet stream of NO gas drives in a single direction to push out the nuclear membrane to form a bubble [13]. Numerous nuclear proteins and nucleoli relocate to the nuclear bubble during BCD [13, 14]. Both actin and α-tubulin are housekeeping proteins. UV rapidly reduces the expression of cytosolic α-tubulin, but has less effect on actin. Intriguingly, cytosolic α-tubulin relocates to the nuclear bubble in UV/cold shock-treated L929S cells, suggesting that nuclear membrane in the bubble leaks. Alternatively, α-tubulin relocates to the bubble through enlarged nuclear pores. In stark contrast, α-tubulin does not undergo relocation to the bubbles of COS7 cells during BCD. The mechanism of this regard is unknown. Compared to control cells, cold shock shrinks and reduces the cell sizes. No apparent structural changes, including shortening or depolymerization, are shown for α-tubulin. In contrast, UV/cold shock-treated cells are shown to have depolymerized α-tubulin.

Whether degradation of α-tubulin occurs is not known. When cultured at 37 ℃, UV-treated cells undergo apoptosis, and α-tubulin appears to be shortened but without relocating to the nuclei.

Finally, by time-lapse holography, we have demonstrated for the first time that there is an increased thickness or height in dividing or apoptotic cells. Cell volume increase occurs normally in dividing cells. The tallness lasts less than 20 min, and then the cell divides. In contrast, during apoptosis, the increased cell height can last for 5 to 8 h, followed by a breakdown of the whole cell. However, during BCD, the bubble released from the nucleus is indeed flattened, compared to the cell body, suggesting that the nuclear bubble contains NO and cytoplasmic liquid. These observations were done with WWOXf L929S and COS7 cells, and whether WWOXd cells tall up before explosion remains to be established.

Conclusions

Our research has uncovered a novel aspect of cell death regulation. We demonstrated the presence of a temperature-sensitive WWOX/TRAF2/p53 complex for regulating UV-mediated cell death, either apoptosis or BCD. UV induces WWOXf cells to undergo BCD and WWOXd cells to undergo POD at low temperatures (less than 22 °C). UV or UV/cold shock induces simultaneous NO production and calcium influx in WWOXf cells, but not in WWOXd cells. Dramatic increases in the cell thickness or height occur during apoptosis at 37 oC, whereas the event did not occur during BCD at low temperatures. UV/cold shock or UV alone downregulates caspase 3, Bak, and α-tubulin, induces relocation of α-tubulin to the nucleus and nuclear bubble, and rapidly reduces housekeeping proteins such as cortactin, α-tubulin and β-actin, thus rendering immobilization of the cells. UV induces co-translocation of the WWOX/TRAF2 complex to the nucleus. At low temperatures, the WWOX/TRAF2 complex dissociates to carry out BCD. At 37 °C, the WWOX/ TRAF2 complex has a strong binding to support apoptosis. Thus, the complex is temperature-sensitive and acts as a molecular switch for either BCD or apoptosis in WWOXf cells.

Abbreviations

BCD	Non-apoptotic nuclear bubbling cell death
DAPI	4′,6-Diamidino-2-phenylindole
DAF-FM (DAF)	(4-Amino-5-Methylamino-2′,7′-Difluorofluorescein Diacetate
DsRed	Red fluorescent protein expressed in the coral genus *Discosoma*
DsRedM	Monomeric DsRed
FRET	Förster resonance energy transfer
HSC70	Heat shock protein 70
MTT	(3-(4,5-Dimethylthiazol-2-yl)-2,5-diphenyltetrazolium bromide
NO	Nitric oxide
NOS2	Nitric oxide synthase 2

POD	Non-apoptotic nuclear explosion or pop-out death
pY33-WWOX	Y33-phosphorylated WWOX
pS14-WWOX	S14-phosphorylated WWOX
SDR domain	Short-chain alcohol dehydrogenase/reductase domain
TRAF2	TNF receptor associated factor 2
TRAF2 domains	Including a Ring (ring-type zinc finger domain), two TRAF zinc finger domains, a CC domain (coiled coil domain), and a MATH (MATH/TRAF) domain

Supplementary Information

The online version contains supplementary material available at https://doi.org/10.1186/s12964-024-01866-6.

Supplementary Material 1.

Authors' contributions
(1) Western blots: C-C Tsai, S-J Chen, S-R Lin; (2) Cell lines and experiments: C-C Tsai, M-H Lee, S-R Lin, H-Y Zeng, L-H Wang, N-S Chang; (3) Time-lapse microscopy: C-C Tsai, N-S Chang; (4) cDNA clones: S-S Huang, M-H Lee, S-R Lin; (5) Manuscript writing and discussion: C-C Tsai, S-J Chen, M-F Chiang, H-M Sheu, N-S Chang; (6) Manuscript revision and discussion: C-C Tsai, S-J Chen, N-S Chang; (7)Antibody production: S-S Huang, M-H Lee, S-R Lin, N-S Chang; (8) Figs. 2, 4, 5, S2, Video S5-S10: C-C Tsai; (9) Figs. 1, 3, S1, S3, S4, Video S1, S2, S3, S4: N-S Chang; (10) Figs. 6 and 7: S-J Chen. All authors have read and agreed to the published version of the manuscript.

Data availability
No datasets were generated or analysed during the current study.

Declarations

Ethics approval and consent for participate
Not applicable.

Consent for publication
Not applicable.

Conflicts of interests
The authors declare no conflict of interest.

Author details
[1]Institute of Molecular Medicine, National Cheng Kung University, Tainan 70101, Taiwan. [2]Graduate Institute of Biomedical Sciences, College of Medicine, China Medical University, Taichung 40402, Taiwan. [3]Chinese Medicine Research Center, Institute of Integrated Medicine, China Medical University, Taichung 40402, Taiwan. [4]Department of Neurosurgery, Fu Jen Catholic University Hospital, Taipei 24352, Taiwan. [5]Department of Dermatology, College of Medicine, National Cheng Kung University, Tainan 70101, Taiwan.

References
1. Chang NS, Hsu LJ, Lin YS, Lai FJ, Sheu HM. WW domain-containing oxidoreductase: a candidate tumor suppressor. Trends Mol Med. 2007;13(1):12–22.
2. Chang JY, Chang NS. WWOX dysfunction induces sequential aggregation of TRAPPC6AΔ, TIAF1, tau and amyloid β, and causes apoptosis. Cell Death Discov. 2015;1:15003.
3. Chen ST, Chuang JI, Wang JP, Tsai MS, Li H, Chang NS. Expression of WW domain-containing oxidoreductase WOX1 in the developing murine nervous system. Neuroscience. 2004;124(4):831–9.
4. Cheng YY, Chou YT, Lai FJ, Jan MS, Chang TH, Jou IM, Chen PS, Lo JY, Huang SS, Chang NS, Liou YT, Hsu PC, Cheng HC, Lin YS, Hsu LJ. *Wwox* deficiency leads to neurodevelopmental and degenerative neuropathies and glycogen synthase kinase 3β-mediated epileptic seizure activity in mice. Acta Neuropathol Commun. 2020;8(1):6.
5. Sze CI, Su M, Pugazhenthi S, Jambal P, Hsu LJ, Heath J, Schultz L, Chang NS. Down-regulation of WW domain-containing oxidoreductase induces Tau phosphorylation in vitro. A potential role in Alzheimer's disease. J Biol Chem. 2004;279(29):30498–506.
6. Chang NS, Pratt N, Heath J, Schultz L, Sleve D, Carey GB, Zevotek N. Hyaluronidase induction of a WW domain-containing oxidoreductase that enhances tumor necrosis factor cytotoxicity. J Biol Chem. 2001;276(5):3361–70.
7. Aldaz CM, Hussain T. WWOX Loss of Function in Neurodevelopmental and Neurodegenerative Disorders. Int J Mol Sci. 2020;21(23):8922.
8. Repudi S, Kustanovich I, Abu-Swai S, Stern S, Aqeilan RI. Neonatal neuronal WWOX gene therapy rescues Wwox null phenotypes. EMBO Mol Med. 2021;13(12): e14599.
9. Kunkle BW, Grenier-Boley B, Sims R, Bis JC, Damotte V, Naj AC, et al. Genetic meta-analysis of diagnosed Alzheimer's disease identifies new risk loci and implicates Aβ, tau, immunity and lipid processing. Nat Genet. 2019;51(3):414–30.
10. Huang SS, Chang NS. Phosphorylation/de-phosphorylation in specific sites of tumor suppressor WWOX and control of distinct biological events. Exp Biol Med (Maywood). 2018;243(2):137–47.
11. Fink SL, Cookson BT. Apoptosis, pyroptosis, and necrosis: mechanistic description of dead and dying eukaryotic cells. Infect Immun. 2005;73(4):1907–16.
12. Proskuryakov SY, Konoplyannikov AG, Gabai VL. Necrosis: a specific form of programmed cell death? Exp Cell Res. 2003;283(1):1–16.
13. Chang NS. Bubbling cell death: A hot air balloon released from the nucleus in the cold. Exp Biol Med (Maywood). 2016;241(12):1306–15.
14. Chen SJ, Lin PW, Lin HP, Huang SS, Lai FJ, Sheu HM, et al. UV irradiation/cold shock-mediated apoptosis is switched to bubbling cell death at low temperatures. Oncotarget. 2015;6(10):8007–18.
15. Hsu LJ, Hong Q, Chen ST, Kuo HL, Schultz L, Heath J, et al. Hyaluronan activates Hyal-2/WWOX/Smad4 signaling and causes bubbling cell death when the signaling complex is overexpressed. Oncotarget. 2017;8(12):19137–55.
16. Chen YA, Sie YD, Liu TY, Kuo HL, Chou PY, Chen YJ, et al. Normal cells repel WWOX-negative or -dysfunctional cancer cells via WWOX cell surface epitope 286–299. Commun Biol. 2021;4(1):753.
17. Chou PY, Lai FJ, Chen YA, Sie YD, Kuo HL, Su WP, et al. Strategies by which WWOX-deficient metastatic cancer cells utilize to survive via dodging, compromising, and causing damage to WWOX-positive normal microenvironment. Cell Death Discov. 2019;5:97.
18. Chang NS, Schultz L, Hsu LJ, Lewis J, Su M, Sze CI. 17beta-Estradiol upregulates and activates WOX1/WWOXv1 and WOX2/WWOXv2 in vitro: potential role in cancerous progression of breast and prostate to a premetastatic state in vivo. Oncogene. 2005;24(4):714–23.
19. Fernandes S, Vieira M, Prudêncio C, Ferraz R. Betulinic Acid for Glioblastoma Treatment: Reality, Challenges and Perspectives. Int J Mol Sci. 2024;25(4):2108.
20. Wimmerová M, Bildziukevich U, Wimmer Z. Selected Plant Triterpenoids and Their Derivatives as Antiviral Agents. Molecules. 2023;28(23):7718.
21. Mu H, Sun Y, Yuan B, Wang Y. Betulinic acid in the treatment of breast cancer: Application and mechanism progress. Fitoterapia. 2023;169: 105617.
22. Chalfant V, Riveros C, Singh P, Shukla S, Balaji N, Balaji KC. Potential role for protein kinase D inhibitors in prostate cancer. J Mol Med (Berl). 2023;101(4):341–9.
23. Ōmura S, Asami Y, Crump A. Staurosporine: new lease of life for parent compound of today's novel and highly successful anti-cancer drugs. J Antibiot (Tokyo). 2018;71(8):688–701.

Chen *et al. Cell Communication and Signaling*   (2024) 22:505

Page 16 of 16

24. Park BS, Abdel-Azeem AZ, Al-Sanea MM, Yoo KH, Tae JS, Lee SH. Staurosporine analogues from microbial and synthetic sources and their biological activities. Curr Med Chem. 2013;20(31):3872–902.

25. Haq R, Zanke B. Inhibition of apoptotic signaling pathways in cancer cells as a mechanism of chemotherapy resistance. Cancer Metastasis Rev. 1998;17(2):233–9.

26. Nicotera P, Leist M, Single B, Volbracht C. Execution of apoptosis: converging or diverging pathways? Biol Chem. 1999;380(9):1035–40.

27. Graczyk PP. Caspase inhibitors as anti-inflammatory and antiapoptotic agents. Prog Med Chem. 2002;39:1–72.

28. Ghazavi F, Huysentruyt J, De Coninck J, Kourula S, Martens S, Hassannia B, et al. Executioner caspases 3 and 7 are dispensable for intestinal epithelium turnover and homeostasis at steady state. Proc Natl Acad Sci U S A. 2022;119(6): e2024508119.

29. Cetraro P, Plaza-Diaz J, MacKenzie A, Abadía-Molina F. A Review of the Current Impact of Inhibitors of Apoptosis Proteins and Their Repression in Cancer. Cancers (Basel). 2022;14(7):1671.

30. Lee D, Long SA, Adams JL, Chan G, Vaidya KS, Francis TA, et al. Potent and selective nonpeptide inhibitors of caspases 3 and 7 inhibitapoptosis and maintain cell functionality. J Biol Chem. 2000;275(21):16007–14.

31. Chen S, Lv X, Hu B, Shao Z, Wang B, Ma K, Lin H, Cui M. RIPK1/RIPK3/MLKL-mediated necroptosis contributes to compression-induced rat nucleus pulposus cells death. Apoptosis. 2017;22(5):626–38.

32. Pawlikowska M, Jędrzejewski T, Brożyna AA, Wrotek S. Protein-Bound Polysaccharides from *Coriolus Versicolor* Induce RIPK1/RIPK3/MLKL-Mediated Necroptosis in ER-Positive Breast Cancer and Amelanotic Melanoma Cells. Cell Physiol Biochem. 2020;54(4):591–604.

33. Liang S, Nian Z, Shi K. Inhibition of RIPK1/RIPK3 ameliorates osteoclastogenesis through regulating NLRP3-dependent NF-κB and MAPKs signaling pathways. Biochem Biophys Res Commun. 2020;526(4):1028–35.

34. Hussain M, Zimmermann V, van Wijk SJL, Fulda S. Mouse lung fibroblasts are highly susceptible to necroptosis in a reactive oxygen species-dependent manner. Biochem Pharmacol. 2018;153:242–7.

35. Chou PY, Lin SR, Lee MH, Schultz L, Sze CI, Chang NS. A p53/TIAF1/WWOX triad exerts cancer suppression but may cause brain protein aggregation due to p53/WWOX functional antagonism. Cell Commun Signal. 2019;17(1):76.

36. Kisselev AF. Site-Specific Proteasome Inhibitors Biomolecules. 2021;12(1):54.

37. Liu T, Sun L, Zhang Y, Wang Y, Zheng J. Imbalanced GSH/ROS and sequential cell death. J Biochem Mol Toxicol. 2022;36(1): e22942.

38. Menichini P, Monti P, Speciale A, Cutrona G, Matis S, Fais F, Taiana E, Neri A, Bomben R, Gentile M, Gattei V, Ferrarini M, Morabito F, Fronza G. Anti-tumor Effects of PRIMA-1 and PRIMA-1(Met) (APR246) in Hematological Malignancies: Still a Mutant P53-Dependent Affair? Cells. 2021;10(1):98.

39. Zatloukalová P, Galoczová M, Vojtěšek B. Prima-1 and APR-246 in Cancer Therapy. Klin Onkol. 2018;31(Suppl 2):71–6.

40. Hientz K, Mohr A, Bhakta-Guha D, Efferth T. The role of p53 in cancer drug resistance and targeted chemotherapy. Oncotarget. 2017;8(5):8921–46.

41. Khamidullina AI, Abramenko YE, Bruter AV, Tatarskiy VV. Key Proteins of Replication Stress Response and Cell Cycle Control as Cancer Therapy Targets. Int J Mol Sci. 2024;25(2):1263.

42. Ronco C, Martin AR, Demange L, Benhida R. ATM, ATR, CHK1, CHK2 and WEE1 inhibitors in cancer and cancer stem cells. Medchemcomm. 2016;8(2):295–319.

43. Hill RL, Singh IN, Brelsfoard J, Hall ED. Pharmacological inhibition of lipid peroxidative damage by the 21-aminosteroid U-74389G improves cortical mitochondrial function following traumatic brain injury in young adult male rats. Neuropharmacology. 2020;170: 108023.

44. Altavilla D, Squadrito F, Campo GM, Squadrito G, Arlotta M, Urna G, Sardella A, Quartarone C, Saitta A, Caputi AP. The lazaroid, U-74389G, inhibits inducible nitric oxide synthase activity, reverses vascular failure and protects against endotoxin shock. Eur J Pharmacol. 1999;369(1):49–55.

45. Luo X, Sedlackova L, Belcastro R, Cabacungan J, Lye SJ, Tanswell AK. Effect of the 21-aminosteroid U74389G on oxygen-induced free radical production, lipid peroxidation, and inhibition of lung growth in neonatal rats. Pediatr Res. 1999;46(2):215–23.

46. Mur LA, Mandon J, Cristescu SM, Harren FJ, Prats E. Methods of nitric oxide detection in plants: a commentary. Plant Sci. 2011;181(5):509–19.

47. Marquet P, Depeursinge C, Magistretti PJ. Review of quantitative phase-digital holographic microscopy: promising novel imaging technique to resolve neuronal network activity and identify cellular biomarkers of psychiatric disorders. Neurophotonics. 2014;1(2): 020901.

48. Schnoor M, Stradal TE, Rottner K. Cortactin: Cell Functions of A Multifaceted Actin-Binding Protein. Trends Cell Biol. 2018;28(2):79–98.

49. Wang Q, Liu X. The dual functions of α-tubulin acetylation in cellular apoptosis and autophage induced by tanespimycin in lung cancer cells. Cancer Cell Int. 2020;20:369.

50. Kamal MA, Al-Zahrani MH, Khan SH, Khan MH, Al-Subhi HA, Kuerban A, et al. Tubulin Proteins in Cancer Resistance: A Review. Curr Drug Metab. 2020;21(3):178–85.

51. Li Z, Yuan W, Lin Z. Functional roles in cell signaling of adaptor protein TRADD from a structural perspective. Comput Struct Biotechnol J. 2020;18:2867–76.

52. Nguyen CN, Urquieta E. Contemporary review of dermatologic conditions in space flight and future implications for long-duration exploration missions. Life Sci Space Res (Amst). 2023;36:147–56.

53. Chang NS, Doherty J, Ensign A. JNK1 physically interacts with WW domain-containing oxidoreductase (WOX1) and inhibits WOX1-mediated apoptosis. J Biol Chem. 2003;278(11):9195–202.

54. Chang NS, Doherty J, Ensign A, Schultz L, Hsu LJ, Hong Q. WOX1 is essential for tumor necrosis factor-, UV light-, staurosporine-, and p53-mediated cell death, and its tyrosine 33-phosphorylated form binds and stabilizes serine 46-phosphorylated p53. J Biol Chem. 2005;280(52):43100–8.

55. Hsu LJ, Schultz L, Hong Q, Van Moer K, Heath J, Li MY, et al. Transforming growth factor beta1 signaling via interaction with cell surface Hyal-2 and recruitment of WWOX/WOX1. J Biol Chem. 2009;284(23):16049–59.

56. Huang SS, Su WP, Lin HP, Kuo HL, Wei HL, Chang NS. Role of WW Domain-containing Oxidoreductase WWOX in Driving T Cell Acute Lymphoblastic Leukemia Maturation. J Biol Chem. 2016;291(33):17319–31.

57. Chen YA, Liu TY, Wen KY, Hsu CY, Sze CI, Chang NS. Zfra Overrides WWOX in Suppressing the Progression of Neurodegeneration. Int J Mol Sci. 2024;25(6):3507.

58. Wang WJ, Ho PC, Nagarajan G, Chen YA, Kuo HL, Subhan D, et al. WWOX Possesses N-Terminal Cell Surface-Exposed Epitopes WWOX(7–21) and WWOX(7–11) for Signaling Cancer Growth Suppression and Prevention In Vivo. Cancers (Basel). 2019;11(11):1818.

59. Su WP, Wang WJ, Chang JY, Ho PC, Liu TY, Wen KY, et al. Therapeutic Zfra4-10 or WWOX7-21 Peptide Induces Complex Formation of WWOX with Selective Protein Targets in Organs that Leads to Cancer Suppression and Spleen Cytotoxic Memory Z Cell Activation In Vivo. Cancers (Basel). 2020;12(8):2189.

60. Chang JY, Lee MH, Lin SR, Yang LY, Sun HS, Sze CI. Trafficking protein particle complex 6A delta (TRAPPC6AΔ) is an extracellular plaque-forming protein in the brain. Oncotarget. 2015;6(6):3578–89.

Publisher's Note